J Mater Sci (2009) 44:6775–6785
DOI 10.1007/s10853-009-3576-7

MESOSTRUCTURED MATERIALS

High selectivity for metal ion adsorption: from mesoporous phosphonated titanias to meso-/macroporous titanium phosphonates

Tian-Yi Ma · Xue-Jun Zhang · Zhong-Yong Yuan

Received: 30 November 2008 / Accepted: 12 May 2009 / Published online: 28 May 2009

Abstract A family of hybrid surface-phosphonated titania, titania–phosphonate, and titanium phosphonate porous materials with different organic groups in the network was synthesized by utilizing a series of organophosphonic acids as the coupling molecules. The crystalline degree of the obtained hybrids decreased by increasing the original added coupling molecule amount, with the structural phase transformed from phosphonated titania to titanium phosphonate, and simultaneously the nanoarchitecture changed from mesoporous to hierarchically meso-/macroporous structure. The whole synthesis process was performed under a very wide pH range by a template-free strategy. The samples were characterized by XRD, N_2 sorption, SEM, TEM, FT-IR, MAS NMR, XPS, and TG-DSC analysis. It is revealed that the integrity of organic groups remained inside the framework of the synthesized hybrids. All the synthesized adsorbents exhibited large capacity of heavy metal ion adsorption with a definite selectivity, which depended on the nature and positions of organically functional groups.

Introduction

The chemically designed inorganic–organic hybrid materials have attracted considerable attention in the recent years because of the combination of properties with respect to the inorganic and the organic components, which allows to tailor density, chemical reactivity, and thermal stability [1]. Metal phosphonates, as an important class of the inorganic–organic hybrid materials, have exhibited extensive applications in the fields of ion exchange, proton conductivity, intercalcation chemistry, and photochemistry [2–4], and the use of organophosphonate derivatives provides an almost unlimited ability to vary the organic component leading to variable modes of functionalization of the solid materials and possible control of the pore size [5]. A large number of hybrid open-framework microporous or mesoporous metal phosphonate materials with various chemical compositions and organic groups have been well documented, showing interesting properties [6, 7], and their applications as catalysts and adsorbents are emerging. Microporous zirconium phosphonates and aluminium phosphonates were constructed from inorganic–organic layers [2, 8–10] through the controlled reactions of diphosphonic acids, phosphoric acid, and metal species. The use of multidentate building blocks, such as amino-bridged tetraphosphonate groups [11], could render the formation of novel zirconium polyphosphonate open-framework compounds with a modular structure, and the dimensions of the cavities/channels inside the structures may be tailored by the right choice of the interlinking organic groups. In addition. the applications of these microporous open-framework metal phosphonates for shape-selective catalyst, separation, and gas storage were also widely reported [2–4].

Meanwhile, the surfactant-templating strategy has recently been utilized for the preparation of mesostructured/mesoporous metal organophosphonate materials. With the use of terminal RPO_3 substituting groups, mesoporous metal phosphate/phosphonate materials were synthesized [12, 13], but the phosphonate incorporation into the final materials is limited and restricted to the pore surface. Kimura

T.-Y. Ma · X.-J. Zhang · Z.-Y. Yuan (✉)
Key Laboratory of Energy-Material Chemistry (Tianjin), Institute of New Catalytic Materials Science, Engineering Research Center of Energy Storage and Conversion (Ministry of Education), College of Chemistry, Nankai Unviersity, Tianjin 300071, People's Republic of China
e-mail: zyyuan@nankai.edu.cn

synthesized ordered mesoporous aluminum organophosphonate by using organically bridged diphosphonic acids ($(HO)_2OP–R–PO(OH)_2$) with limited types of alkylene-bridged groups in the presence of either alkyltrimethylammonium surfactant [14, 15] or oligomeric surfactant or triblock copolymer [16], but their possible applications have not been reported yet. Haskouri et al. [17] synthesized mesoporous aluminum phosphonates and diphosphonates from aluminum atrane complexes and methylphosphonic and/or ethylenediphosphonic acids. Vasylyev et al. prepared titanium and vanadium phosphonate materials with irregular porosity by a non-hydrolytic condensation of metal alkoxide with a dendritic tetraphosphonate [18, 19], which could catalyze oxidation of benzylic alcohols under aerobic conditions [18]. However, the homogeneous incorporation of phosphonate units into mesoporous metal oxide networks is still a challenge as regards their application potential [20, 21].

Heavy metal ions, especially mercury and lead, are highly toxic environmental pollutants. A series of organic–inorganic hybrid mesostructured/mesoporous silica-based adsorbents have been developed for removal of heavy metal ions from waste streams [22, 23], where the organic functionalities in these adsorbents typically serve to form complexes with heavy metal ions through acid–base reactions, and the solid support allows easy removal of the loaded adsorbent from the liquid waste. Thiols, thiourea, and amines have been used as metal ion-binding motifs for the efficient removal of toxic heavy metals like Hg(II), Cu(II), and Cd(II) [22–25]. However, phosphonated metal oxide or metal phosphonate materials for heavy metal ion adsorption was little investigated. Our efforts were invested in the designed synthesis of functionalized mesoporous and meso-/macrostructured metal oxide–phosphonate and metal phosphonate hybrid materials for highly selective adsorption [26–29]. The template-free preparation of mesoporous phosphonated titanias, hierarchical meso-/macroporous titania–diphosphonate hybrids, and titanium tetraphosphonate materials was performed. The porous hierarchy and the nature of hybrid materials could be tunable by the nature of the coupling phosphonic acid molecules and their amount added. The obtained hybrid adsorbents were found to show their significant adsorption capacity with high adsorption selectivity, indicating promising adsorbents for metal ion recovery and environmental remediation.

Experimental section

Materials preparation

1-Hydroxy ethylidene-1,1-diphosphonic acid (HEDP), ethylenediamine tetra(methylene phosphonic acid) (EDTMPS), and diethylenetriamine penta(methylene phosphonic acid) (DTPMPA) were used as coupling phosphonate molecules for titania–phosphonate hybrid (TiO_2–PPh), titanium phosphonate (TiPPh), and surface-phosphonated titania (PPh–TiO_2), respectively. A calculated amount of the phosphonic acid was added into a mixed solution of 30 mL of deionized water and 15 mL of ethanol, followed by dropwise addition of 0.005 mol of tetrabutyl titanate. After a further stirring of 24 h, the obtained mixture was sealed in one teflon-lined autoclave and aged statically at 80 °C for 24 h. The product was filtered, washed with water, and dried at 60 °C. The phosphonic acid/tetrabutyl titanate mole ratios were 1/4, 2/4, and 3/4 for PPh–TiO_2, TiO_2–PPh, and TiPPh, respectively. The pH value of the reaction solution was adjusted to between 5 and 10.5 by adding HCl or NaOH solution. Pure mesoporous titania was synthesized by the similar procedure in the absence of phosphoric acid for comparison.

Characterization

Scanning electron microscopy (SEM) and transmission electron microscopy (TEM) were carried out on a Shimadzu SS-550 microscope at 15 keV and a Philips Tecnai G20 at 200 kV, respectively. N_2 adsorption–desorption isotherms were recorded on a Quantachrome NOVA 2000e sorption analyzer at liquid nitrogen temperature (77 K). The samples were degassed at 100 °C overnight prior to the measurement. The surface area was obtained by the Brunauer–Emmett–Teller (BET) method, and pore size distribution was calculated from the adsorption branch of the isotherm by the Barret–Joyner–Halenda (BJH) model. Fourier transform infrared (FT-IR) spectra were measured on a Bruker VECTOR 22 spectrometer with KBr pellet technique, and the ranges of spectrograms were 4,000–400 cm^{-1}. X-ray diffraction (XRD) patterns were recorded on a Rigaku D/max-2500 diffractometer with CuK_α radiation operated at 40 kV and 100 mA. Thermogravimetry (TG) and differential scanning calorimetry (DSC) were performed using a Setaram DTA92-16.18 instrument at a heating rate of 5°/min using α-Al_2O_3 as the reference. The chemical compositions of Ti and P were analyzed by inductively coupled plasma (ICP) emission spectroscopy on a Thermo Jarrell-Ash ICP-9000 (N + M) spectrometer, and C, N, and H were analyzed on a Vario-EL elemental analyzer. Solid-state ^{31}P and ^{13}C magic angle spinning (MAS) nuclear magnetic resonance (NMR) spectra were recorded on a Varian Unity plus-400 spectrometer at spinning rates of 12 and 6 kHz and resonance frequencies of 161.9 and 100.5 MHz with recycle time of 5 and 3 s, and the chemical shifts were referenced to H_3PO_4 (85% in water) and tetramethylsilane (TMS), respectively.

Metal ion adsorption

Heavy metal ion adsorption tests of the hybrid mesoporous materials were performed in batch mode. Adsorbents weighing 0.01 g were added into 50 mL of homoionic solution containing different concentrations (10, 20, and 30 mg/L) of $Cu(NO_3)_2$, $Cd(NO_3)_2$, or $Pb(NO_3)_2$. The mixture was stirred for 3 h, followed by centrifugation at 6,000 rpm for 15 min. For Cu^{2+} ion adsorption, 20 mL of obtained clear solution, A mixture of 12 mL of ethanol and 30 mL of dicyclohexanoneoxalyldihydrazone solution (0.4 g of dicyclohexanoneoxalyldihydrazone solved in 50 mL of ethanol and then adjusted to 500 mL with water) was made up to 100 mL by adding more water, and allowed to adjust with ammonia to pH = 8–9, which is the best pH value for chromogenic reaction. The volume of Cu(II) adsorbed was monitored by measuring the UV absorption at $\lambda_{max} = 600$ nm of the initial and final solutions. For Cd^{2+} and Pb^{2+} adsorption, 1-(2-pyridinylazo)-2-naphthanol and diphenylthiocarbazone were used as chromogenic reagents, respectively, and average loading capacities and efficiency were also monitored by UV-vis spectroscopy at λ_{max} (Cd^{2+}) = 555 nm and λ_{max} (Pb^{2+}) = 480 nm. Notably, solubilizing agents (surfactants or emulsifiers) were necessary for the chromogenic reaction of Cd^{2+} and Pb^{2+}.

Results and discussion

Synthesis and characterization of hybrid materials

The preparation of porous surface-phosphonated titania, titania–diphosphonate, and titanium phosphonate materials was performed in a mixed solution of water and ethanol by a spontaneous assembling process without addition of any templates, and different kinds of phosphonic acids were used as organophosphorus coupling molecules. The key to control the final material phase, whether crystalline, semicrystalline, or amorphous phase, is to adjust the molar ratio of the original added coupling molecules and the tetrabutyl titanate. The crystalline degree of the obtained hybrids decreased with the structural phase transformed from phosphonated titania to titanium phosphonate, by increasing the original added coupling molecule amount, and simultaneously the nanoarchitecture also changed from mesoporous to hierarchically meso-/macroporous structure, as it can be seen in Figs. 1 and 2. The XRD pattern of PPh–TiO_2 (Fig. 1a) gives typical peaks at 2θ values of 25.1°, 38.0°, 47.8°, 54.8°, 63.1°, 69.2°, and 75.1°, which were evident for the presence of a crystalline anatase structure. The pure TiO_2 sample prepared by the similar method without the phosphonic acid addition shows an additional peak at 2θ of 30.6°, indicating a bicrystalline structure of anatase and brookite (not shown herein) [30]. The crystallite sizes of PPh–TiO_2 and pure TiO_2, calculated by the Scherrer formula, are 4.2 and 9.5 nm, respectively. It is seen that the crystalline size dramatically decreased for PPh–TiO_2 sample, indicating that the organophosphonate incorporation efficiently prevented the formation of brookite phase and the growth of the particle size. The XRD pattern of the synthesized TiO_2–PPh (Fig. 1b) presents several very weak diffraction peaks that could be identified as anatase phase. This indicates that the hydrolysis of titanium alkoxide in the phosphonic acid solution resulted in the incorporation of organophosphonate in the titania network, suggesting semicrystalline anatase

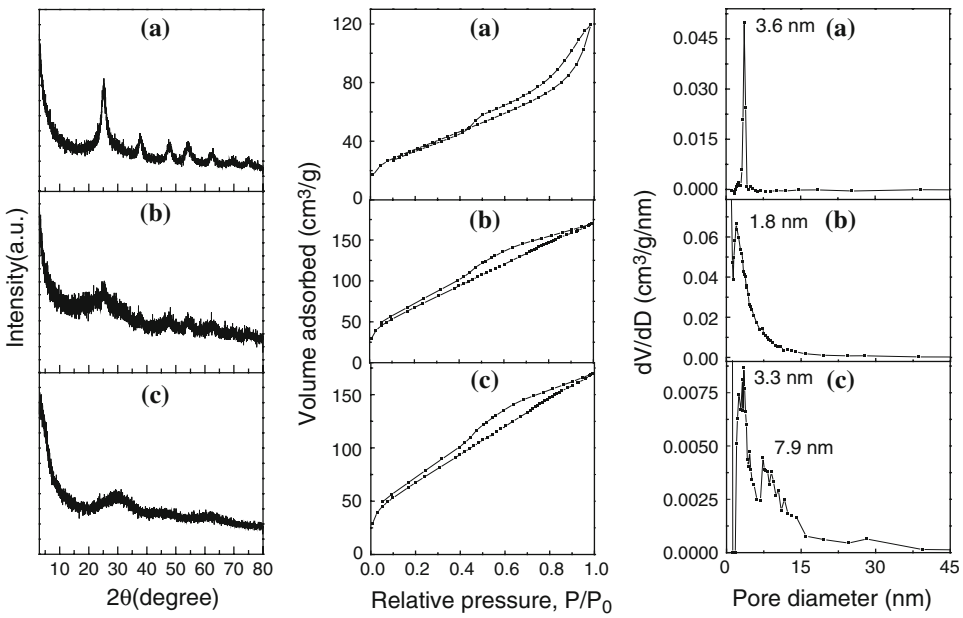

Fig. 1 Wide-angle XRD patterns (*left*), nitrogen adsorption–desorption isotherms (*middle*) with corresponding BJH pore size distribution curves (*right*) of the synthesized hybrid adsorbents: (**a**) PPh–TiO_2[DTPMPA]; (**b**) TiO_2–PPh[HEDP], and (**c**) TiPPh[EDTMPS]

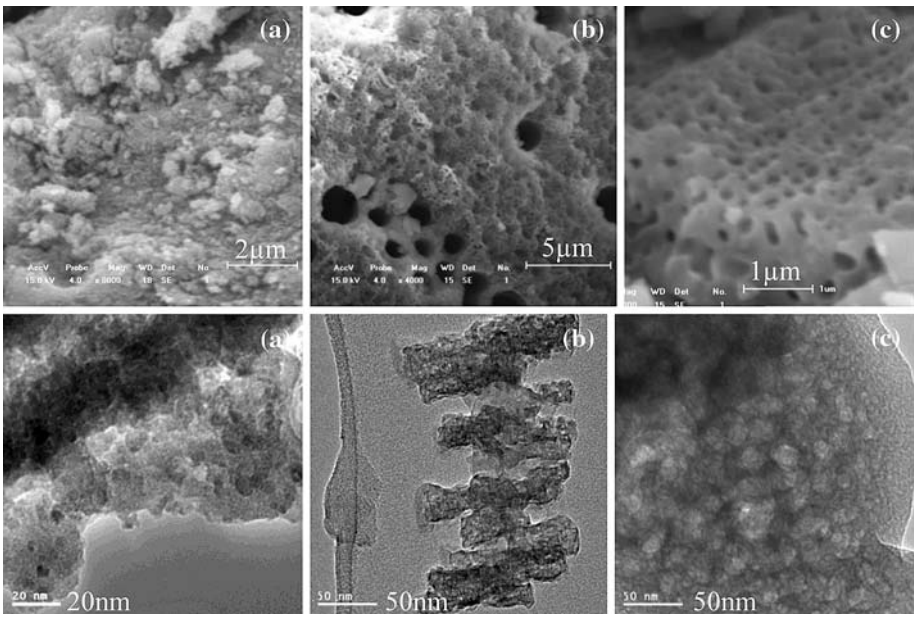

Fig. 2 SEM (*up*) and TEM (*down*) images of the synthesized hybrid adsorbents: **a** PPh–TiO_2[DTPMPA]; **b** TiO_2–PPh[HEDP], and **c** TiPPh[EDTMPS]

nanoparticles of about 3 nm in size linked each other with amorphous titanium phosphonate nanoclusters. The TiPPh sample possesses amorphous framework walls, as revealed by powder XRD pattern in Fig. 1c. No crystalline $TiPO_4$ or TiO_2 phases appear. Further, no low-angle diffraction peaks were observed, indicating the nonexistence of a long-range order of mesopore arrays in these hybrid materials.

The nitrogen adsorption–desorption isotherms of the obtained samples are quite different (Fig. 1). The isotherm of PPh–TiO_2 (Fig. 1a) is of between type II and type IV, much closer to type II, having a gradual increase of nitrogen-adsorbed volume at high P/P_0 region, showing the presence of a small amount of larger mesopores with disordered channels, which have been observed previously in several as-synthesized (surfactant-containing) mesoporous silica materials [31, 32]. A small hysteresis loop of type H3 is seen in these hybrids, indicating these surface-phosphonated titania materials comprising aggregates (loose assemblages) of platelike particles forming narrow slitlike pores [33]. Single narrow peak centered at 3.6 nm was observed in the corresponding pore size distribution curves (determined by the BJH method from the adsorption branch of the isotherm), and the surface area was measured to be 158 m^2/g, based on the 10-point Brunauer–Emmett–Teller (BET) method, which are lower than that of the pure TiO_2 (245 m^2/g), indicative of the effect of the organic phosphonate incorporation in the titania network. The isotherm of TiO_2–PPh (Fig. 1b) is of type II, having a gradual increase of nitrogen-adsorbed volume with the increase of relative pressure, which have been observed previously in some macroporous materials [31]. The adsorption and desorption branches of the isotherm do not coincide, which is due to the existence of the organic species and the effect of pore connectivity. The pore size distribution curve derived from the adsorption branch of the isotherm using the BJH method exhibits an asymmetric peak maximized at 1.8 nm, suggesting the irregular mesostructure in the TiO_2–PPh hybrid. The multi-point BET surface area is 257 m^2/g with a total pore volume of 0.26 cm^3/g. The isotherm of TiPPh (Fig. 1c) is of between type IV and type II, with a large hysteresis loop, characteristic of mesoporous structure with good pore connectivity. The pore size distribution curve derived from the adsorption branch of the isotherms shows one narrow peak in the range of 2–5 nm, centered at 3.3 nm, and one broad distribution at 6–15 nm. The BET surface area is low of only 15 m^2/g, possibly because of the existence of the organic species.

The SEM image of the synthesized mesoporous PPh–TiO_2 hybrid (Fig. 2a) indicates that it is in irregular shape of aggregate, composed of the very small granular particles of around tens of nanometers, and its TEM images reveal the presence of disordered wormhole-like mesopores in these hybrids, which is the result of the well-defined agglomeration of the granular or platelike particles with the size of tens of nanometers. The lattice fringes of titania can be seen in the high-resolution image, reflecting the crystalline phase of the nanoparticles. Figure 2b shows the SEM and TEM images of the synthesized TiO_2–PPh. A large number of alveolate macropores with openings ranging from 90 to 400 nm spread over the whole particles, among which several huge macrochannels with diameters in micrometer scale (mainly 1–3 μm) are interspersed. The macroporous frameworks were composed of uniform nanorods of 80–150 nm in length and 18–38 nm in thickness, and wormhole-like disordered mesostructures were

also observed in these nanorods. The SEM and TEM images of the resultant TiPPh solid are shown in Fig. 2c, revealing a hierarchically macro-/mesoporous structure presented in the irregular-shaped product particles of tens to several tens of micrometers in size. A uniformly arranged macroporous structure with pore sizes of hundreds of nanometers (100–300 nm) is clearly observed from the SEM images, which is further confirmed by the TEM images. The walls between the macropores are mainly of 200–450 nm in thickness, composed of mesostructured pores of several nanometers in size with wormhole-like assembly in the area near the pore surface layers, revealed by the high-magnification TEM images. In the core part of the macroporous walls and under the particle/pore surface layers of small wormhole-like mesoporous structure, a novel mesocellular foam structure, similar to the previously reported mesostructured cellular foam (MCF) silica materials [34], was seen. The bimodal mesopore size distributions of 2–5 and 6–15 nm calculated from the nitrogen adsorption analysis should correspond to the wormhole-like mesostructure and mesocellular foam structure observed in TEM images, respectively. The formation of the wormhole-like mesoporous structures of these hybrid materials should follow a mechanism of nanoparticle assembly [26], which is distinct with the surfactant-templating of ordered mesostructures. The formation of hierarchical meso-/macroporous structures of TiO_2–PPh and TiPPh might be related to the presence of the microemulsion system during the hydrolysis of tetrabutyl titanate precursors in organophosphonic acid solution under mild stirring to form nanometer-sized titanium phosphonate sols, titanium oxo cluster, as well as nanosized titania–phosphonate particles, giving a multiple component system of alkoxide/organophosphonate–alcohol (butanol, ethanol)–water [35]. The interfacial microemulsion polymerization of titanium phosphonate sols and titanium oxo clusters rendered the formation of mesostructured titania–phosphonate nanorods with homogenously attached organophosphonate units or the mesocellular foam structure of titanium phosphonate nanoparticles. These further aggregated along with the microemulsions to give a hierarchical macroporous structure by microphase separation; the nature of organophosphonate may assume an important role in the feature of hierarchical meso-/macroporous structure, since it could affect deeply the microemulsion system generated.

The XRD, nitrogen adsorption analysis, and electron microscopy results have thus clearly revealed that by adjusting the phosphonic acid/tetrabutyl titanate molar ratio from 1/4 to 2/4 to 3/4, the structural phases of the obtained materials transformed from crystalline surface-phosphonated titania to semicrystalline titania–phosphonate hybrid to amorphous titanium phosphonate, and the porous hierarchy changed from disordered mesoporous structure to hierarchically meso-/macroporous structure, suggesting the structural controllability effect in these hierarchical porous hybrid materials.

In order to investigate the influence of acidity of the reaction solution on the morphologies and porosities of these hybrid materials, the preparation process of TiPPh was carried out in a much wider pH range. When the synthesis was performed in the weak acid system by adding HCl, e.g., pH = 5, an alternative macro-structure of TiPPh[EDTMPS] solid was obtained (Fig. 3), exhibiting a sandwich-like hierarchy with dense surface layers and macroporous cores. Careful examination of these SEM micrographs (Fig. 3b, d) reveals that the walls of the macroporous cores are composed of worm-eaten channels, together forming a three-dimensional network. On further lowering the pH values to pH = 1–3, only irregular-shaped particles without macroporous structures were obtained. Increasing the pH value of the synthesis solution by adding NaOH, for example, at pH = 10–13, rather irregular macrovoids were obtained in the resultant solids. It should be noted that the pH value of the synthesis system strongly affected the morphology of the resultant titanium phosphonate materials. The reaction rates of the hydrolysis of titanium alkoxide and condensation of titanium organophosphonate species were accelerated in the strong acid or alkali solution, which would lead to the unwanted aggregation before the microphase-separated domains of Ti-phosphonate-based nanoparticles and water/alcohol channels, which is the main cause of the changeable macroporosity. The aggregation would prevent the generation of macropores, which might be the reason why the well-structured macropores could be only obtained in the mild near-neutral solution system (pH = 5–8). The nitrogen adsorption–desorption isotherms and the corresponding pore size distributions of TiPPh[EDTMPS] samples prepared at different pH values are shown in Fig. 4. The adsorption–desorption isotherms of all the TiPPh samples synthesized at different pH values are of between type IV and type II, characteristic of mesoporous structure with good pore connectivity. The pore width distribution curve estimated using the Density functional theory (DFT) shows one narrow peak in the range of 2–5 nm, and one broad distribution at 7–9 nm. These two kinds of mesopore size distributions correspond to the wormhole-like mesostructure and mesocellular foam structure observed in TEM images (Figs. 1c and 3e), respectively. It is quite notable that the surface area and pore volume increase, while the pore width decreases with the increasing of the acidity of reaction solutions. The sample prepared at pH = 5 possesses the highest surface area of 86 m^2/g, while the BET surface area of the sample prepared at pH = 10.5 is the lowest, namely, only 4 m^2/g, possibly because of the existence of the organic species.

The ^{31}P and ^{13}C MAS NMR spectra of the PPh–TiO_2[DTPMPA] sample are shown in Fig. 5a. The ^{31}P

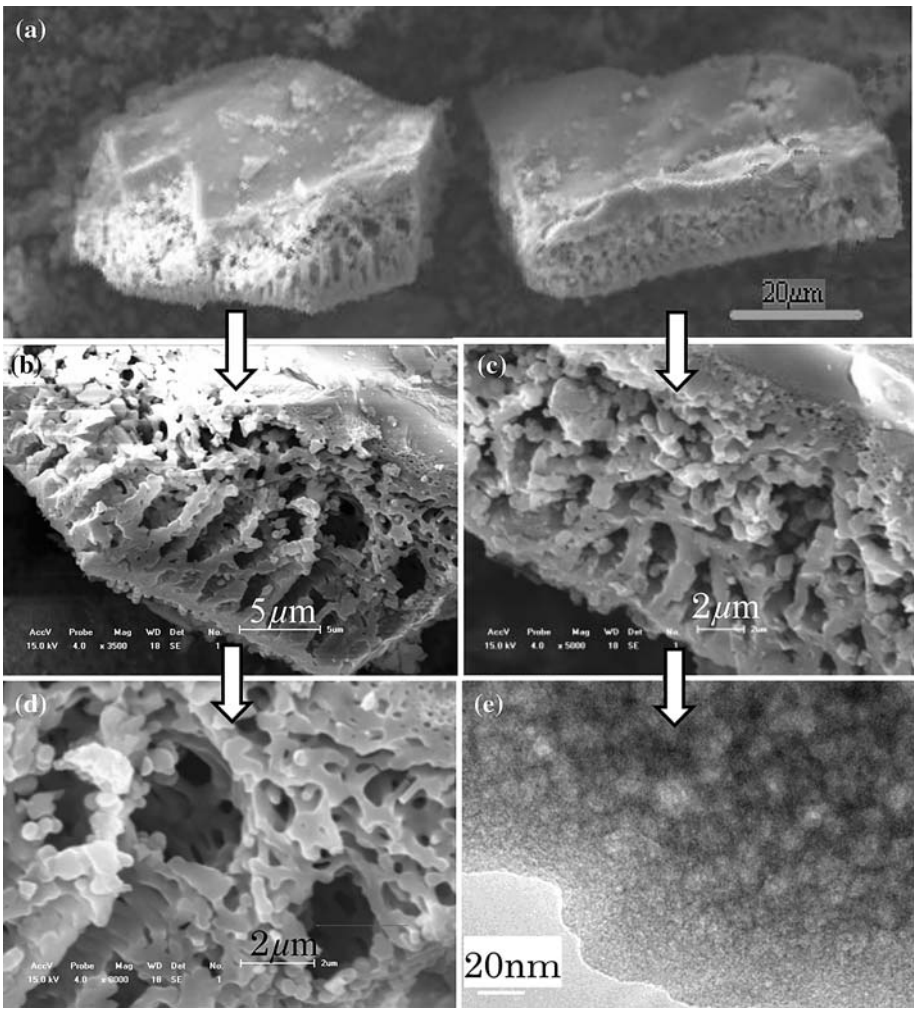

Fig. 3 **a–d** SEM and **e** TEM images of the sandwich-like hierarchical TiPPh[EDTMPS] sample synthesized under pH = 5

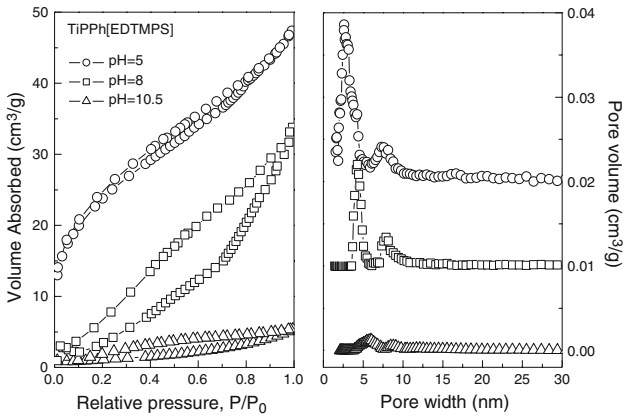

Fig. 4 N_2 adsorption–desorption isotherms and the corresponding pore width distribution curve determined by DFT method, of the meso-/macroporous TiPPh[EDTMPS] synthesized at pH = 5, pH = 8 and pH = 10.5, and the pore volume was shifted by 0.02, 0.01 and 0, respectively

MAS NMR spectrum shows one broad signal around 8 ppm, which is in the area characteristic of phosphonates. The broadening of the resonance signal is due to the disordered or low-crystalline nature of solids. This signal has the similar chemical shifts found for Ph*P*$(OTi)_3$ units in molecular oxo phosphonato titanium clusters of phenylphosphonate-TiO_2 hybrids [20] and for diphosphonate groups ($\equiv$P–CH_2–P$\equiv$) in mesoporous aluminum phosphonates [14–16]. No sharp ^{31}P NMR resonance signal at −4 ppm was observed, indicating that a layered titanium phosphonate phase [18–20] was not present in the synthesized materials. ^{13}C MAS NMR spectrum shows a major signal at 53 ppm, corresponding to the carbon atoms in nitrilomethylenephosphonate groups. These suggest that no phase separation took place during the preparation of the hybrid samples, and DTPMPA groups were dispersed homogeneously within a TiO_2 network. ^{31}P MAS NMR spectrum of the resultant TiO_2–PPh[HEDP] sample shows the resonance at 16 ppm (Fig. 5b), which can be attributed to diphosphonate groups ($\equiv$P–C(OH)(CH_3)–P$\equiv$) linked to the Ti atoms [14, 15, 28], and ^{13}C MAS NMR spectrum of the sample exhibits the resonances at 20 and 69 ppm, which correspond to the C atoms of the terminal CH_3 group and the quaternary carbon atom connected with the P=O

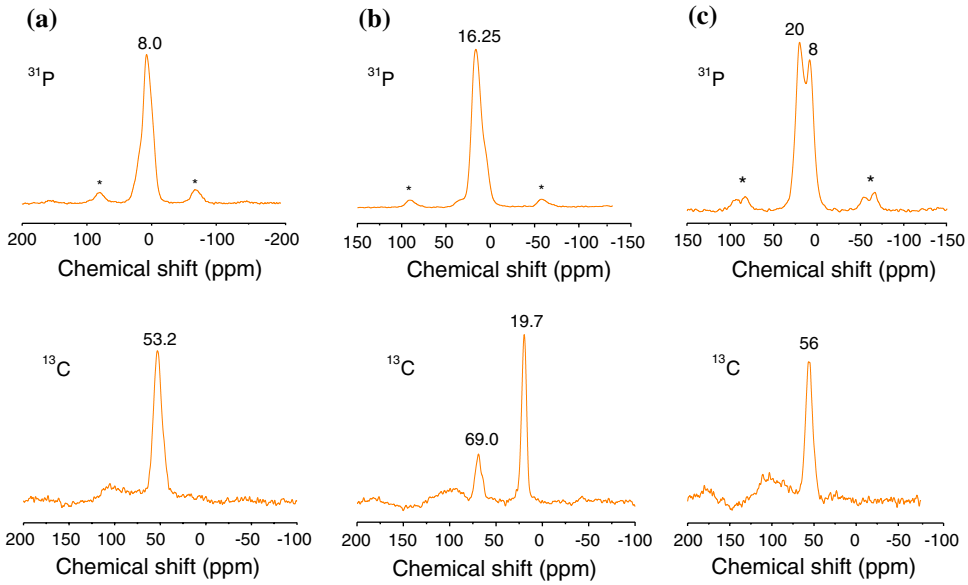

Fig. 5 ^{31}P and ^{13}C MAS NMR spectra of synthesized samples: **a** PPh–TiO_2[DTPMPA]; **b** TiO_2–PPh[HEDP] and **c** TiPPh[EDTMPS]

group of the phosphonate, respectively. ^{31}P and ^{13}C MAS NMR spectra of hierarchical meso-/macroporous TiP-Ph[EDTMPS] are shown in Fig. 5c. The ^{31}P MAS NMR spectrum shows two resonance signals of the phosphorus nuclei at 20 and 8 ppm, which could be assigned to P atoms of RPO_3H^- and RPO_3^{2-}, respectively. ^{13}C MAS NMR spectrum of the sample shows the somewhat broadened signal around 56 ppm, corresponding to the carbon atoms of nitrilomethylene and ethylenediamine in the framework of phosphonate groups. These data suggest that organophosphonate groups retain their integrity in the porous solid.

Figure 6 shows the high-resolution XPS spectra of Ti 2p, P 2p and O 1s, taken on the surface of the PPh–TiO_2, TiO_2–PPh and TiPPh materials. The Ti 2p line of PPh–TiO_2[DTPMPA] sample is composed of two single peaks situated at 457.3 eV for Ti $2p_{3/2}$ and 463 eV for Ti $2p_{1/2}$. Compared with the binding energy of pure TiO_2 (459 eV for Ti $2p_{3/2}$ and 464.8 eV for Ti $2p_{1/2}$), the binding energy of main Ti 2p decreases in the phosphonated titania hybrids, which results from the organophosphonate incorporation in the titania network. The P 2p broad line could be fitted into two peaks around 133.6 and 131.5 eV. This indicates that in PPh–TiO_2[DTPMPA], a part of the phosphonate groups was not connected with titania but exposed on the titania surface, because of the claw-type structure of big pentaphosphonate DTPMPA molecules, though the surface atomic ratio of P/Ti was calculated as 1. No peak appears at 128.6 eV, which is the characteristic binding energy of P in TiP [36], indicating the absence of Ti–P bonds in our mesoporous phosphonated titania materials. The broad O 1 s signals at 529.7 eV were observed, which are ascribed to the oxygen co-contributed from Ti–O, P–O and P=O bonds and for TiO_2–PPh[HEDP], the Ti 2p line is composed of two single peaks situated at 459.4 eV for Ti 2p3/2 and 465.2 eV for Ti 2p1/2, which are characteristic of Ti^{4+}. The P 2p binding energy is observed around 133.1 eV, characteristic of P^{5+} in phosphonate groups, and the broad O 1s signal might be fitted by four components, situated at 530.7, 531.4, 532.1, and 533.0 eV, ascribed to the oxygen contributed from Ti–O, P–O, O–H, and C–O bonds, respectively [37]. The XPS spectra of TiPPh material were also similar to that of PPh–TiO_2 and TiO_2–PPh (Fig. 6c), due to the similar nature of Ti, P, C, and O species in these mateirals.

The thermal stability of the synthesized hybrids were determined by the thermal gravimetric analysis (TGA) and differential scanning calorimetry (DSC), and the results are shown in Fig. 7. Figure 7a is the TG-DSC profiles of the sample PPh–TiO_2[DTPMPA]. The TGA curves demonstrate initial weight loss of 18.1% from room-temperature to 260 °C, accompanied with a endothermal peak around 110 °C in the DSC curve, which may be assigned to the desorption of the adsorbed and intercalated water. The weight losses of 12.3% from 260 to 900 °C, accompanied with two exothermic peaks at around 320 and 750 °C, can be attributed to the decomposition of the organic species and the coke combustion. Figure 7b and c shows the TG-DSC profiles of TiO_2–PPh[HEDP] and TiPPh[EDTMPS], respectively, revealing their similar thermal behaviors with PPh–TiO_2[DTPMPA].

The ICP emission spectroscopy was employed to analyze chemical compositions (P, Ti) of the resultant solids. Combined with the conventional elemental analysis of C, H, and N, the chemical compositions could be formulated as $C_{3.6}H_{7.2}O_6N_{1.3}P_{1.8}(TiO_2) \cdot xH_2O$ for PPh–TiO_2[DTPMPA] (experimental 6.41% Ti, 7.33% P, 5.78% C, 3.81% H, and 2.40% N in mass), $(TiO_2)C_2H_4O_5P_2 \cdot xH_2O$ for TiO_2–

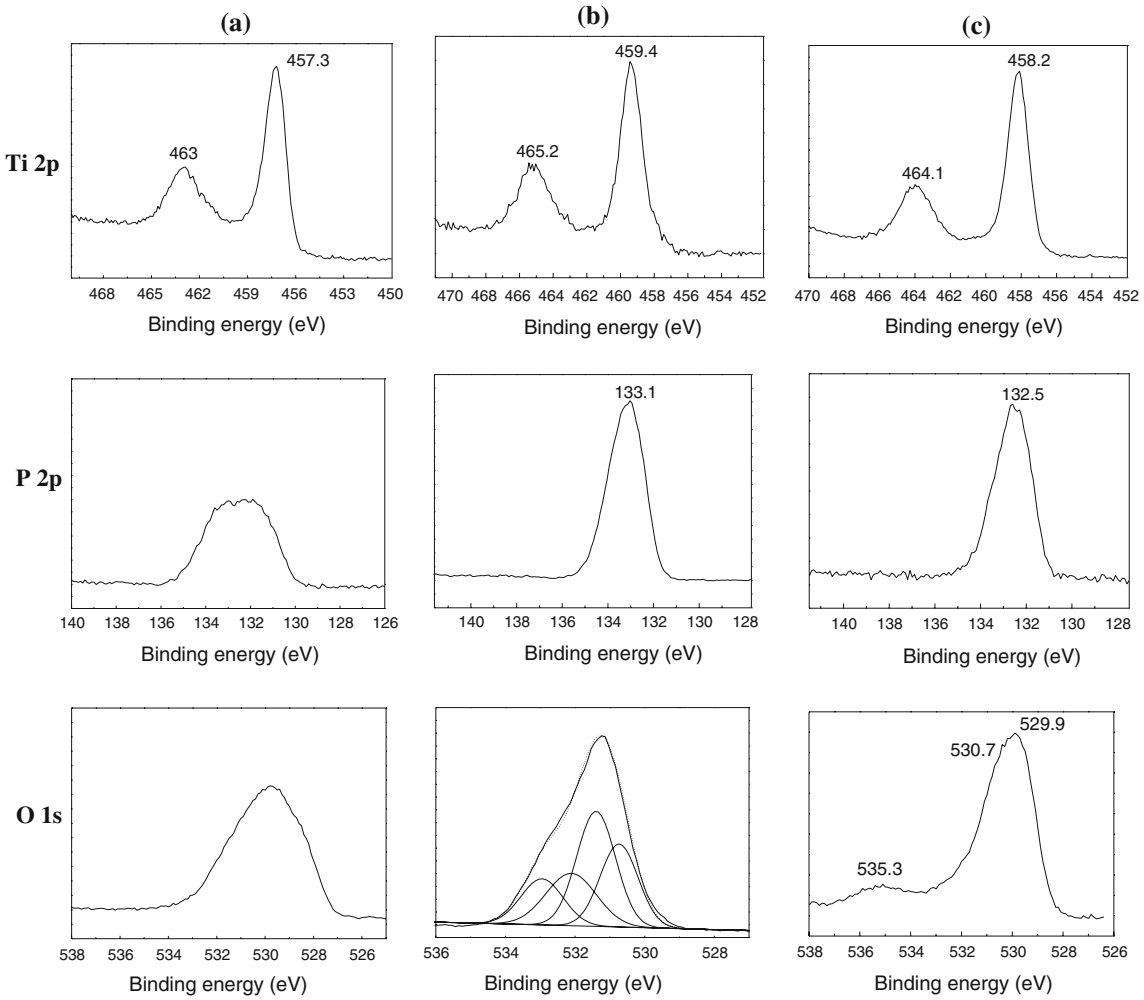

Fig. 6 High-resolution XPS spectra of the Ti 2p, P 2p and O 1 s regions of **a** PPh–TiO_2[DTPMPA]; **b** TiO_2–PPh[HEDP] and **c** TiPPh[EDTMPS]

PPh[HEDP] (experimental 15.55% Ti, 12.31% P, 6.03% C, and 5.29% H in mass), and $Ti(C_3H_6O_6NP_2) \cdot xH_2O$ for TiPPh[EDTMPS] (experimental 8.30% Ti, 10.76% P, 6.24% C, and 5.31% H in mass).

Heavy metal ion adsorption of the hybrid adsorbents

The potential of the synthesized surface-phosphonated titania, titania–phosphonate and titianium phosphonate hybrid adsorbents to remove the heavy metal ions Cd(II), Cu(II), and Pb(II) from independent homoionic solutions was tested, and the adsorption efficiency results are summarized in Fig. 8. Moreover, by using the equation [22, 25] $K_d = (c_i - c_f)V_{soln}/(c_f m_{ads})$, the distribution coefficient (K_d) (Fig. 9) could also be determined, where c_i is the initial metal ion concentration, c_f is the ion concentration after adsorption, V_{soln} is the volume of the solution (in mL), and m_{ads} is the amount of adsorbent (in g). It is seen that the adsorption efficiency of all the hybrid adsorbents for Cd(II), Cu(II), and Pb(II) ions are higher than pure TiO_2, which proves that the observed ion concentration change is indeed attributed to the complexation reactions between metal ions with grafted ligands other than surface area and porous structure. It is interesting to note that a significant higher binding ability for Cd(II) with the best results up to 88.75 and 89.17% was observed in the PPh–TiO_2 [DTPMPA] and PPh–TiO_2[EDTMPS] samples, respectively, while only 7.08% for pure TiO_2 even when the initial concentration of Cd(II) was 10 mg/L. Notably, the tendency for different initial concentration of metal ion was similar for each sample, that is, the adsorption efficiencies increased with the decrease of the initial concentrations of metal ions, clearly demonstrating that the samples appeared to essentially tend to their high loading capacity in low metal ions concentration. The K_d values of PPh–TiO_2 for Cu(II), Cd(II) and Pb(II) are all higher than that TiO_2, while the K_d values for Cd(II) adsorbed onto the synthesized adsorbents (22,000–40,400 mL/g) are much higher than for Cu(II) (810–2300 mL/g) and Pb(II) (300–760 mL/g). This demonstrates the remarkable selectivity of

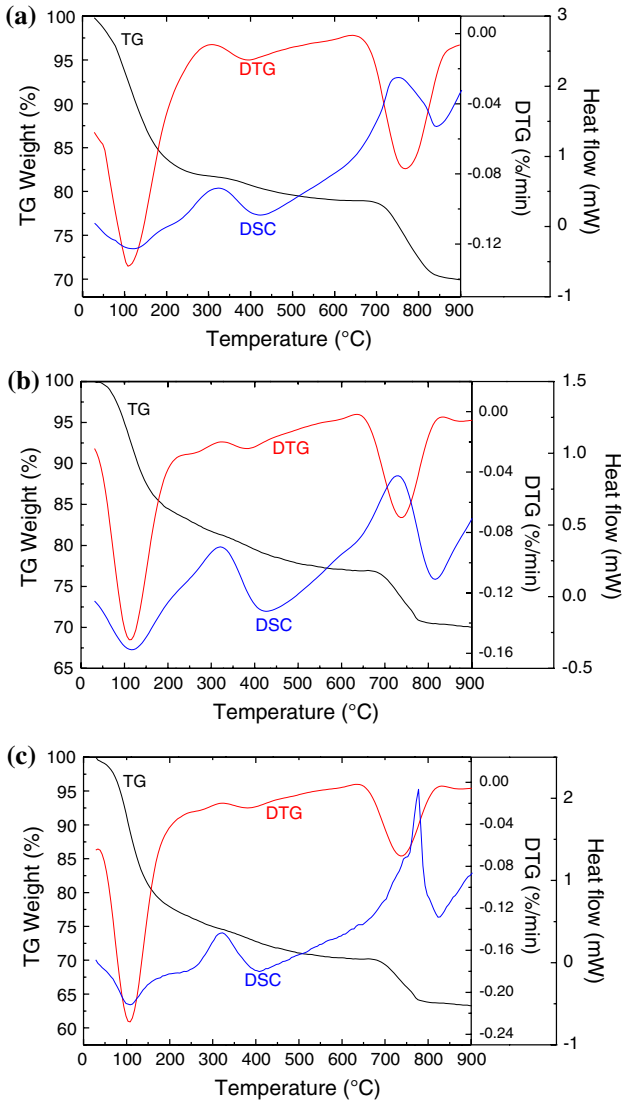

Fig. 7 TG-DSC profiles of the hybrid adsorbents: **a** PPh–TiO_2 [DTPMPA]; **b** TiO_2–PPh[HEDP] and **c** TiPPh[EDTMPS]

PPh–TiO_2 adsorbents for Cd^{2+} (Fig. 9). It is really of great significance since the previously reported organic-functionalized mesoporous silicas exhibited very weak complexation affinity for Cd^{2+} [24]. The competitive adsorption experiment was also performed by treating a mixed ionic solution containing Pb(II) (10 mg/L), Cu(II) (10 mg/L), and Cd(II) (10 mg/L) with PPh–TiO_2. The residual concentrations of the metal ions were determined by chromogenic reaction and spectrophotometry, similar to that of Cu^{2+}. The coincident result was also obtained by AES method (atomic emission spectroscopy). The adsorption capacities of 0.011 mmol/g Pb(II), 0.073 mmol/g Cu(II), and 0.102 mmol/g Cd(II) were obtained. This again proved a distinct preference of the mesoporous phosphonated titania adsorbants for the uptake of Cd^{2+} ions compared to that of Cu^{2+} and Pb^{2+}, indicating that the synthesized mesoporous PPh–TiO_2 materials have an innate specificity for the adsorption of Cd^{2+} over Cu^{2+} and Pb^{2+}. On the contrary, the selective complexation affinity sequence for metal ions of TiO_2–PPh adsorbents is Cd(II) < Pb(II) < Cu(II), and the adsorption efficiency for Cd^{2+} ions ranged from 23.45% to 26.67%, for Pb^{2+} ions ranged from 31.92% to 39.09%, and for Cu^{2+} ranged from 37.62% to 57.55%, which are far higher than that of the pure TiO_2. The distribution coefficient (K_d) values of 2344–3208 mL/g, 3015–6708 mL/g, and 1531–1818 mL/g were also determined for TiO_2–PPh in the adsorption of Pb^{2+}, Cu^{2+}, and Cd^{2+}, respectively, while only 200–400 mL/g were obtained for pure TiO_2. The much higher K_d values of TiO_2–PPh than pure TiO_2 indicate the efficiently increased affinity of the organic–inorganic hybrid sorbent for the metal ion adsorption.

The adsorption efficiency of the TiPPh[EDTMPS] for Cd^{2+} ions ranged from 72.13 to 77.92%, for Pb^{2+} ions ranged from 84.62 to 90.91%, and for Cu^{2+} ranged from 83.33 to 85.85%, which are far higher than that of the pure TiO_2 prepared in the absence of organophosphonates. The selective complexation affinity sequence of metal ions is Cd(II) < Cu(II) < Pb(II) for TiPPh. In order to test the reusability of the hierarchical titanium phosphonate adsorbents, the Cu^{2+} ion loaded TiPPh[EDTMPS] sample, taken as representative, was treated with 1 mol/L hydrochloric acid for 8 h to remove the heavy metal ions and then neutralized, subsequent to a second round of metal ion adsorption testing. The results for Cu^{2+} ion adsorption using the regenerated adsorbents are summarized in Fig. 10. Only a little decrease of the adsorption efficiency was seen in the second use, and the samples retain their Cu^{2+} uptake capacities of 76.82% after four multi-use cycles. Then, the Cu^{2+} uptake capacities decreased gradually in the next successive uses, but the materials still retain greater than 56% of the original metal ion loading capacity after leaching nine times. This suggests the stability of the synthesized hierarchical titanium organophosphonate materials and the retention of their adsorption properties under the relatively strong acid leaching conditions, making them useful as reusable sorbents for multiple metal ion adsorption cycles. The observed high adsorption ability of inorganic–organic hybrid adsorbents is mainly caused by the bridged phosphonates containing ligands for binding metal ions, including the =N–, –OH and P–O of the coupling phosphonic acid. Cu-loaded hybrid adsorbent was characterized by the UV–vis diffuse-reflectance spectroscopy, in which a sharp fall of absorbance between 300 and 350 nm can be seen, while a broad shoulder appears ranging from 700 to 900 nm. The phenomenon is also related to the Cu complex on the surface of the materials [22], and inorganic–organic framework is playing the most important role in providing coordination sites.

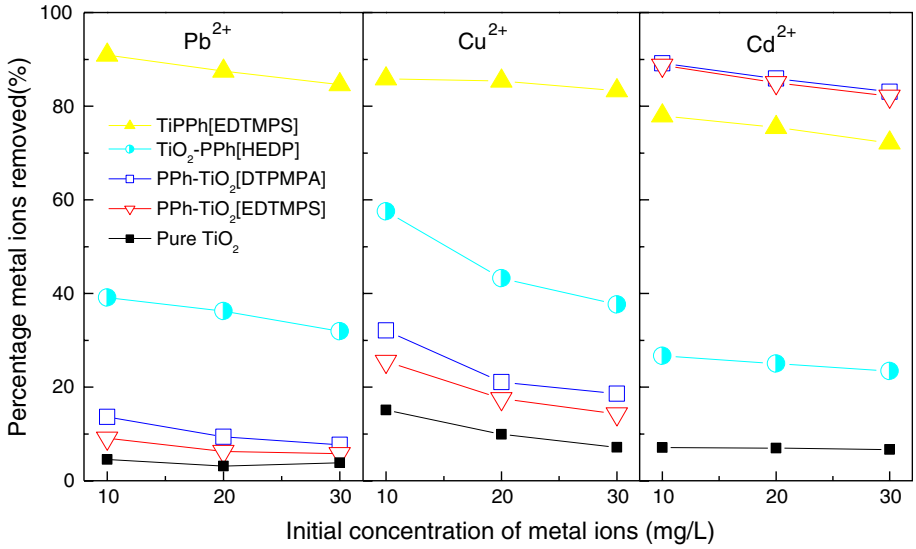

Fig. 8 Metal ion adsorption efficiency for hybrid adsorbents, compared with pure TiO_2

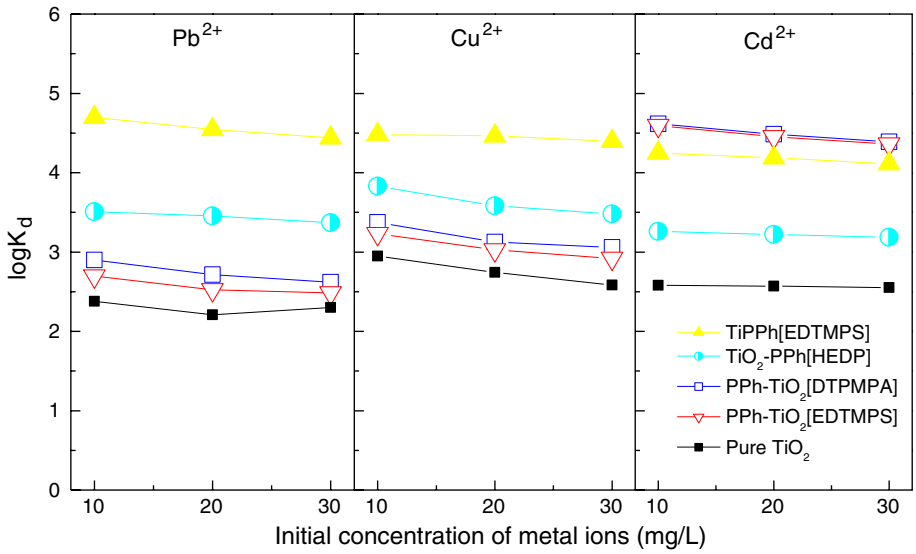

Fig. 9 Distribution coefficient (K_d) profiles for the hybrid adsorbents, compared with pure TiO_2

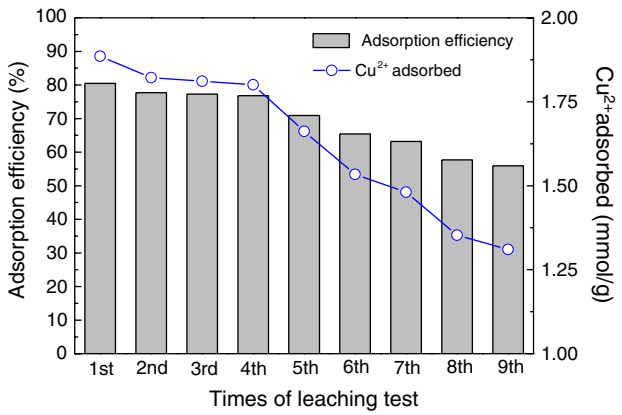

Fig. 10 Reusability of the adsorbent TiPPh[EDTMPS] (synthesized at pH = 8) for Cu^{2+} (30 mg/L) adsorption

Conclusions

Mesoporous surface-phosphonated titania, hierarchically meso-/macroporous titania–phosphonate and titanium phosphonate hybrid adsorbents have been prepared by a simple template-free nanoparticle-assembly procedure with the use of different kinds of organophosphonic acids as the coupling molecules. With the increase of the molar ratio of the original added phosphonic acid and tetrabutyl titanate, the structural phase transformed from crystalline phosphonated titania to semicrystalline titania–phosphonated hybrid to amorphous titanium phosphonate, and simultaneously the nanoarchitecture also changed from disordered mesoporous to hierarchically meso-/macroporous structure. The pH value of the synthesis system also strongly affected

the morphology and textural property of the resultant hybrid materials. The selective complexation affinity with different metal ions on different hybrid adsorbents depends on the nature and positions of organically functional groups in the synthesized samples. Mesoporous organophosphonated titanias exhibited unique selective complexation affinity for Cd^{2+} with the sequence of $Pb^{2+} < Cu^{2+} < Cd^{2+}$, and titania–phosphonate showed a selective complexation affinity for Cu^{2+} with the sequence of $Cd^{2+} < Pb^{2+} < Cu^{2++}$, while hierarchical meso-/macroporous titanium phosphonates with intraframework ethylenediamine groups exhibited large capacity for all the three kinds of ion adsorption with a preference sequence of $Cd^{2+} < Cu^{2+} < Pb^{2+}$ and effective regeneration ability.

Acknowledgements This study was supported by the National Natural Science Foundation of China (No. 20473041 and 20673060), the National Basic Research Program of China (No. 2009CB623502), the Specialized Research Fund for the Doctoral Program of Higher Education (20070055014), the Natural Science Foundation of Tianjin (08JCZDJC21500), the Program for New Century Excellent Talents in University (NCET-06-0215), and Nankai University.

References

1. Sanchez C, Soler-Illia GJdeAA, Ribot F, Lalot T, Mayer CR, Cabuil V (2001) Chem Mater 13:3061
2. Clearfield A, Wang Z (2002) J Chem Soc Dalton Trans 15:2937
3. Maeda K (2004) Microporous Mesoporous Mater 73:47
4. Clearfield A (1996) Curr Opin Solid State Mater Sci 1:268
5. Clearfield A (2002) Curr Opin Solid State Mater Sci 6:495
6. Rosi NL, Eckert J, Eddaoudi M, Vodak DJ, Kim J, O'Keeffe M, Yaghi OM (2003) Science 300:1127
7. Kitagawa S, Kondo M (1998) Bull Chem Soc Jpn 71:1739
8. Clearfield A, Wang JD, Tian Y, Stein E, Bhardwaj C (1995) J Solid State Chem 117:275
9. Alberti G, Costantino U, Marmottini F, Vivani R, Zappelli P (1993) Angew Chem Int Ed Engl 32:1357
10. Kazuyuki M, Yoshimichi K, Fujio M (1994) Angew Chem 106:2427
11. Vivani R, Costantino F, Costantino U, Nocchetti M (2006) Inorg Chem 45:2388
12. Ren N, Tang Y, Wang Y, Hu S, Dong A, Hua W, Yue Y, Shen J (2002) Chem Lett 1036
13. Shi X, Yang J, Yang Q (2006) Eur J Inorg Chem 1936
14. Kimura T (2003) Chem Mater 15:3742
15. Kimura T (2005) Chem Mater 17:337
16. Kimura T (2005) Chem Mater 17:5521
17. Haskouri JEl, Guillem C, Latorre J, Beltrán A, Beltrán D, Amorós P (2004) Eur J Inorg Chem 9:1804
18. Vasylyev M, Neumann R (2006) Chem Mater 18:2781
19. Vasylyev M, Wachtel EJ, Popovitz-Biro R, Neumann R (2006) Chem Eur J 12:3507
20. Guerrero G, Mutin PH, Vioux A (2000) Chem Mater 12:1268
21. Guerrero G, Mutin PH, Vioux A (2001) J Mater Chem 11:3161
22. Dai S, Burleigh MC, Shin Y, Morrow CC, Barnes CE, Xue Z (1999) Angew Chem Int Ed Engl 38:1235
23. Liu AM, Hidajat K, Kawi S, Zhao DY (2000) Chem Commun 1145
24. Brown J, Mercier L, Pinnavaia J (1999) Chem Commun 69
25. Dai S, Burleigh MC, Ju YH (2000) J Am Chem Soc 122:992
26. Zhang XJ, Ma TY, Yuan ZY (2008) J Mater Chem 18:2003
27. Zhang XJ, Ma TY, Yuan ZY (2008) Eur J Inorg Chem 2721
28. Ma TY, Zhang XJ, Shao GS, Cao JL, Yuan ZY (2008) J Phys Chem C 112:3090
29. Zhang XJ, Ma TY, Yuan ZY (2008) Chem Lett 37(7):746
30. Shao GS, Zhang XJ, Yuan ZY (2008) Appl Catal B 82:208
31. Kruk M, Jaroniec M, Ryoo R, Joo SH (2000) Chem Mater 12:1414
32. Park M, Komarneni S (1998) Microporous Mesoporous Mater 25:75
33. Kruk M, Jaroniec M (2001) Chem Mater 13:3169
34. Schmidt-Winkel P, Lukens WW, Zhao DY, Chmelka BF, Yang PD, Stucky GD (1999) J Am Chem Soc 121:254
35. Yuan ZY, Ren TZ, Su BL (2003) Adv Mater 15:1462
36. Baunack S, Oswald S, Scharnweber D (1998) Surf Interface Anal 26:471
37. Ren TZ, Yuan ZY, Azioune A, Pireaux JJ, Su BL (2006) Langmuir 22:3886